Automatika

Journal for Control, Measurement, Electronics, Computing and Communications

ISSN: (Print) (Online) Journal homepage: https://www.tandfonline.com/loi/taut20

# Experimental validation of solar PV sustained ZSI based unified active power filter for enrichment of power quality

S. Parthiban & Vijayakumar Madhaiyan

**To cite this article:** S. Parthiban & Vijayakumar Madhaiyan (2021) Experimental validation of solar PV sustained ZSI based unified active power filter for enrichment of power quality, Automatika, 62:1, 137-153, DOI: 10.1080/00051144.2021.1908013

**To link to this article:** https://doi.org/10.1080/00051144.2021.1908013



Published online: 30 Mar 2021.

AUTOMATIKA
2021, VOL. 62, NO. 1, 137–153
https://doi.org/10.1080/00051144.2021.1908013



# Experimental validation of solar PV sustained ZSI based unified active power filter for enrichment of power quality

S. Parthiban [a] and Vijayakumar Madhaiyan [b]

[a]Electrical and Electronics Engineering Department, Nandha College of Technology, Erode, India; [b]Electrical and Electronics Engineering Department, K.S.R. College of Engineering, Namakkal, India

**ABSTRACT**

The deployment of power electronic devices has become a big concern for power quality in these days. The voltage stabilization of power distribution networks interconnected with Photo Voltaic (PV) is very critical in promoting the smooth operation of all linked devices in the distribution system. Voltage profile maintenance is one of the challenges in PV integration into the grid. Conventional devices such as passive filters, series and shunt filters, synchronous condensers, etc. are insufficient to alleviate numerous problems of power quality. The series compensator is used for voltage quality and the shunt compensator is used for current quality. Also, if these two problems of power quality are simultaneously mitigated, the device is used in the distribution system known as Unified Active Power Filter (UAPF). The shunt and series compensator of UAPF is equipped with a Z-source inverter(ZSI). This paper addresses voltage and current associated existing power quality concerns which including voltage sag, voltage swell, voltage and current distortion and simulates the UAPF device to alleviate these problems. The Unit Vector Template Generation (UVTG) with Improved Second Order Generalized Integrator (ISOGI) based Phase Locked Loop (PLL) is utilized for UAPF controller simulation and experimental results validated the proposed work.

**ARTICLE HISTORY**
Received 18 January 2020
Accepted 19 November 2020

**KEYWORDS**
Photovoltaic system; unified active power filter; Z-source inverter; unit vector template generation; power quality

## 1. Introduction

The electric apparatus has been very vulnerable to numerous problems of power quality. Problems of power quality result in serious economic or production losses. Many devices, such as a computer, uninterrupted power supply, drives, etc. are key factors of power quality problems. The issues of power quality will impact both the utility grid and other customers connected at the end of utility[1]. As a consequence, researchers focus on power quality to minimize different power quality issues, to the obvious benefit of consumers and utilities respectively[2,3]. Quality of power implies efficiency of voltage and current quality since the two parameters strive with the majority of issues of electricity supply[4]. Voltage issues include voltage sag, voltage swell, voltage interruption, transient/notching, voltage distortion, etc. while current related issues include reactive power burden, voltage regulation, and harmonic current owing to non-linear loads, etc[5]. Voltage slope and swell emerged while strong loads in the network were suddenly turned on or off. Voltage sag and swell emerged while large loads in the network were suddenly turned on or off. This tends to lead to equipment failure and loss of data. The first technique is the series and shunt passive filters, which mitigate problems in terms of power quality[6,7]. Though acceptable results have been obtained, issues with design limitations and system resonance with the use of passive filters have induced researchers to detract from active power filters. The study indicates the two main types of active power filters, that is to mention series active power filters and shunt active power filters. The series active filter mitigates all power quality concerns correlated with voltage whereas the shunt active power filter is used for all current associated power quality issues[8,9].

The UAPF is a combination of active power filters linked back to back within a typical DC-link both in series and parallel connection. It also concurrently mitigates all voltage-dependent and current associated device problems[10]. The power quality demonstrates the quality of voltage and reliability of the frequency[11]. According to IEEE 1159 std, if the voltage value in the Root Mean Square (RMS) is between 10 and 90% of the nominal magnitude, then it is considered voltage sag for 0.5 power cycle to 1 min. Documentation of control methods suggested in the literature, including Synchronous Reference Theory (SRF), Instantaneous Reactive Power Theories (IRPT), Unit Vector Template Generation (UVTG), etc., are used to mitigate power quality issues and numerous

**CONTACT** M. Vijayakumar mvijayksrce@gmail.com Electrical and Electronics Engineering Department, K.S.R. College of Engineering, Tiruchengode, Namakkal 637 215, India

problems with power efficiency, related current and voltage[12,13]. In general, an interconnected PV network with a traditional grid is a two-stage system. The first step is for the DC-DC boost converter to step-up voltage and the same is to be converted in AC with an inverter[14]. The efficiency is lower due to two power conversion stages and the total cost of the system is also increasing[15]. A single-stage approach is designed to overcome these drawbacks of the two-stage approach. The PV system produced power transmits directly to the load in a single-stage PV system with a steady reference voltage through the DC – link condenser of the inverter in a regulated manner[16]. An appropriate PV array output voltage is usually needed on the DC side of the inverter for these single-stage PV systems[17]. In the voltage source inverter (VSI) based interconnected PV network, the DC-side voltage should be more than 450 V to reach the phase-voltage of 230 V on the side of the AC. Numerous solutions have been developed to incorporate a broad range of PV arrays into the grid using a single conversion method. The grid-connected inverters for PV incorporation are generally used[18]. In this research work, the author intends to alleviate the shortfall through the development of UAPF s using Z-source inverters for both series and shunt compensators for PV integration to the utility grid[19]. The development is that a 3-phase UAPF is being proposed for PV integration using a Z-source inverter with an energy storage unit[20]. The shunt compensator consumes the active power oscillatory component and injects the active power of the PV source and compensates the load reactive power and device reactive losses. The configuration is cost-efficient, despite low DC-link voltage, limited storage volume of the energy storage system, low capacity for PV network voltage and low inverter capacity[21]. In the laboratory with the FPGA controller, a prototype UAPF model with Z-source inverter is established and the outcomes are confirmed.

The review of the associated works indicates that traditional converters are not desirable. By using the ZSI, the inverter output voltage can be boosted and reduced. Due to this incomparable ability, the ZSI will operate shoot-through-state. The PV-UAPF topology based on ZSI therefore seems very optimistic. Moreover, the traditional UAPF, assisted by DC-links with storage condensers or battery storage modules, cannot provide long-term compensations for distortions dependent on current and voltage. With the ISOGI control algorithm the suggested PV-supported ZSI-UAPF has the following impressive capabilities:

- The ISOGI algorithm offers effective filtering, better stable conditions and quicker response and less complexity in applying this.
- The improved SOGI control algorithm has good capabilities for filtering and increased flexibility and adaptive responses and is easy to implement.
- This control system responds rapidly and preserves the voltage and current profile for a changing source and load conditions.
- The ZSI-UAPF interfaced with the PV system avoids the use of cascading DC-DC converters, used in traditional PV-UAPF. In the prototype model, ZSI is used to increase the PV array output voltage to retain the UAPF DC bus to compensate for the long-term distortions of voltage and current.
- With the implementation of multi-mode functional ability, it manages the various circumstances efficiently and provides continuous clean power for the sensitive load.
- ZSI-UAPF stabilizes the load voltage and retains the load power needed even under serious failure conditions.

The remaining sections of this article are presented as follows. Section 2 presents the Z-source network-based UAPF topology. In Section 3, series compensator control and shunt compensator control are presented. Then, the experimental results and discussion for different case studies are presented in Section 4. Finally, Section 5 concludes the paper.

## 2. Z-source network-based UAPF topology

Figure 1 displays the 3-phase UAPF circuit diagram with a Z-source inverter. The source is modelled on the system of 400 V, three-phase. Due to its special circuit topology, the Z-source inverter acts as a buck–boost inverter, without utilizing a DC-DC converter. The key function of the shunt compensator system is to provide reactive current to suppress THD in current and terminal voltages. If no reactive current is taken from the source unity power factor can be achieved. The reference current can only be obtained if the source is required to include real power and losses. The series compensator is used to alleviate distribution network voltage sag and swell.

Three operating states are included in the planned PV-interfaced UAPF. The operating states are (1) PV power generation (2) Power backup (3) Uninterrupted supply. The operating modes work according to the key parameters such as PV output power($P_{PV}$), supply voltage ($V_S$) and State of Charging (SOC) of battery.

(1) PV power generation

During the day time when solar radiation is far more available for electricity production, the PV power generation state is enabled. ZSI-UAPF assisted by PV is used to compensate harmonics and reactive power and the battery storage device store excess energy produced by the PV system. This mode works based on the PV output power and SOC of the battery. The control flow

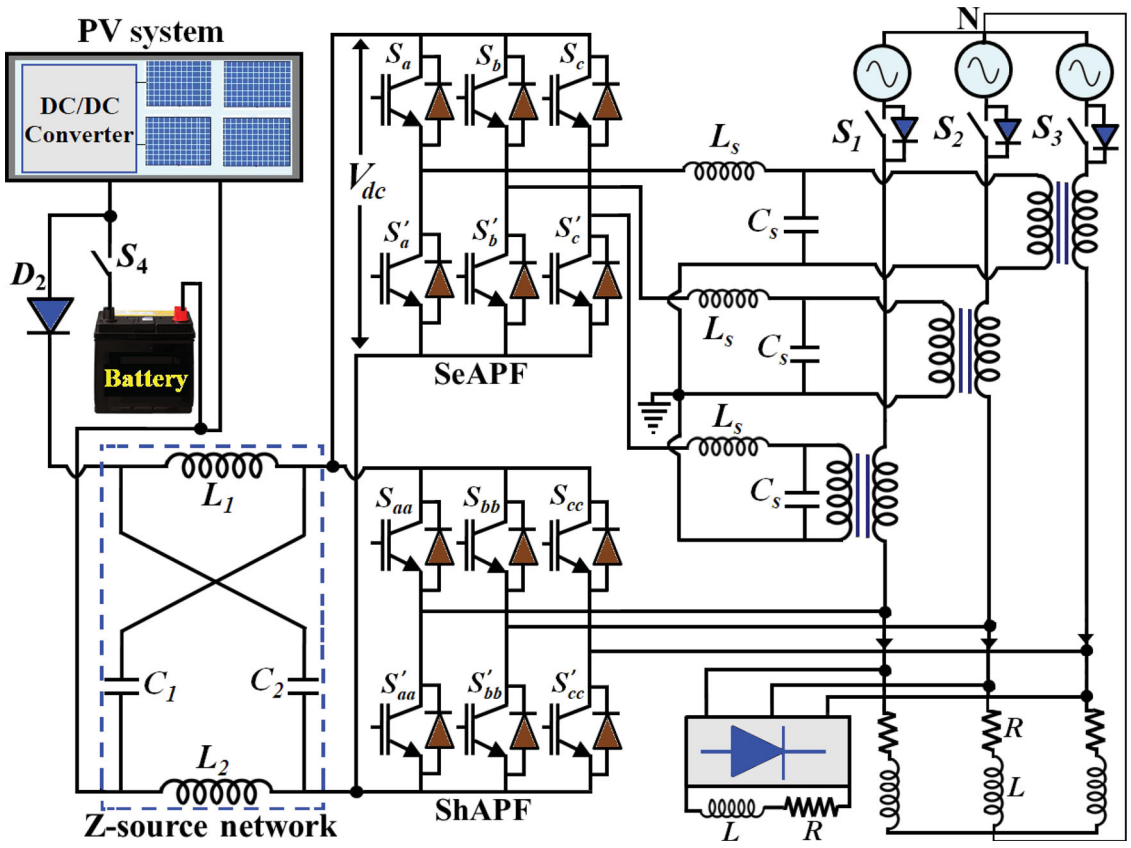


**Figure 1.** The 3-phase UAPF circuit diagram with a Z-source inverter.

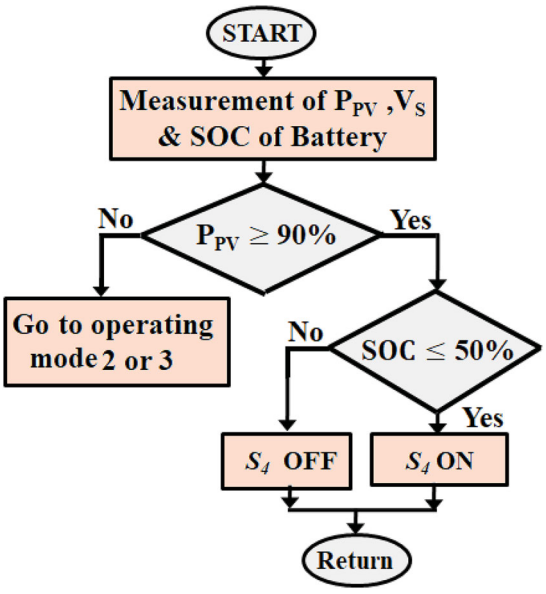


**Figure 2.** Control flow diagram for the PV power generation state.

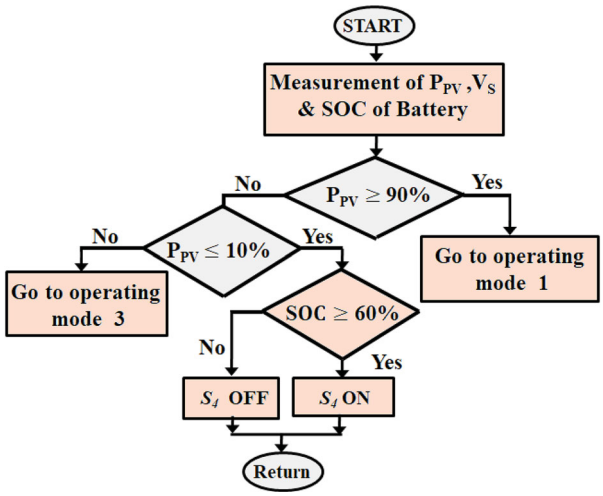


**Figure 3.** Control flow diagram for the power backup state.

diagram for the PV power generation state is shown in Figure 2.

(2) Power backup

The power backup state is activated through the usage of a battery storage device at night or when solar irradiation is inaccessible. The battery-powered ZSI-UAPF compensates for the harmonics and reactive power burden. The mode is facilitated based on the PV power output and the battery SOC. The battery backup mode is achieved through ZSI to maintain the continuity of the compensation effectively. Figure 3 shows the control flow diagram for the power backup state.

(3) Uninterrupted supply

In the voltage disruption period, the SPV-UAPF model offers a continuous supply of essential and sensitive loads. During these instances, either the solar PV power

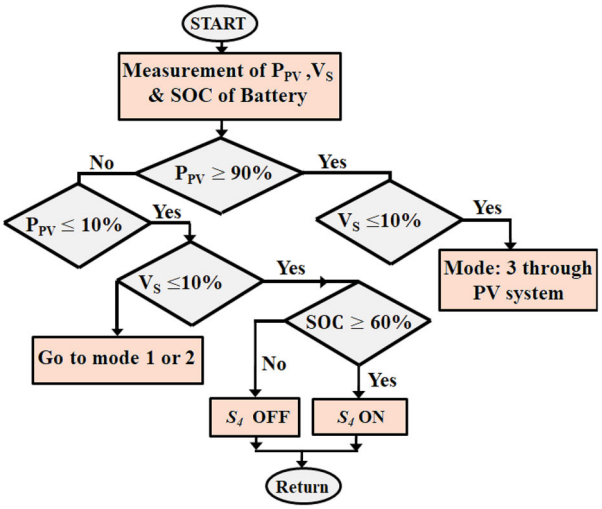


**Figure 4.** Control flow diagram for the uninterrupted supply state.

generation unit or the battery supplies the power source to the attached load. Semiconductor switches isolate the power supply source of the distribution system. The control flow diagram for the uninterrupted supply state is shown in Figure 4.

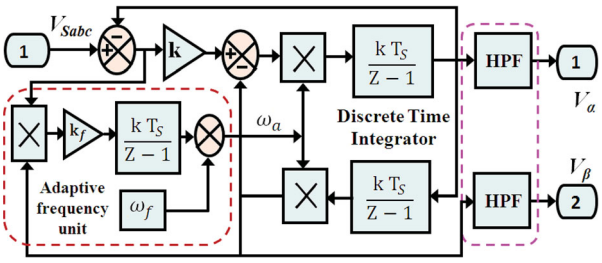


**Figure 5.** An internal configuration of ISOGI-PLL

## 3. Control strategy of ZSI-UAPF

The ZSI-UAPF uses UVTG and ISOGI based PLL to provide compensation in the current and voltage of the distribution system. Dynamically, and effectively, the SOGI method reduces noise, but frequency signal feedback is needed during the orthogonal signal processing phase for the normal oscillation frequency. The phase-locking accuracy of SOGI based PLL remains inadequate due to DC compensation, harmonic disruption and frequency shifts[22]. DC removal PLL processes based on a changed SOGI architecture are established, to add filters. The system's dynamic characteristics can be improved and DC elimination can be accomplished. Both the adaptive frequency unit and the High Pass Filter (HPF) are connected to the improved SOGI. Figure 5 shows the internal configuration of ISOGI-PLL. The ISOGI transfer functions can be attained as

$$f_1(s) = \frac{V_\alpha(s)}{V_{sabc}(s)} = \frac{k\,\omega\, s}{s^2 + k\,\omega\, s + \omega^2} \quad (1)$$

$$f_2(s) = \frac{V_\beta(s)}{V_{sabc}(s)} = \frac{k\,\omega^2}{s^2 + k\,\omega\, s + \omega^2} \quad (2)$$

Let $V_{Sabc}$ represents source voltage (V), damping coeficient is indicated by $k$, $\alpha$ reference frame component of voltage is denited by $V\alpha$, the $\beta$ reference component of voltage is represented by $V_\beta$, and the resonant frequency (rad/s)is indicated by $\omega$.

The orthogonal signals in the ISOGI-PLL are obtainable by introducing a closed-loop configuration for DC offset rejection in standard SOGI-PLL. This decreases the transfer function DC gain to zero by inserting an additional filter element. The influence of DC offset in the output was therefore reduced. In this case, the

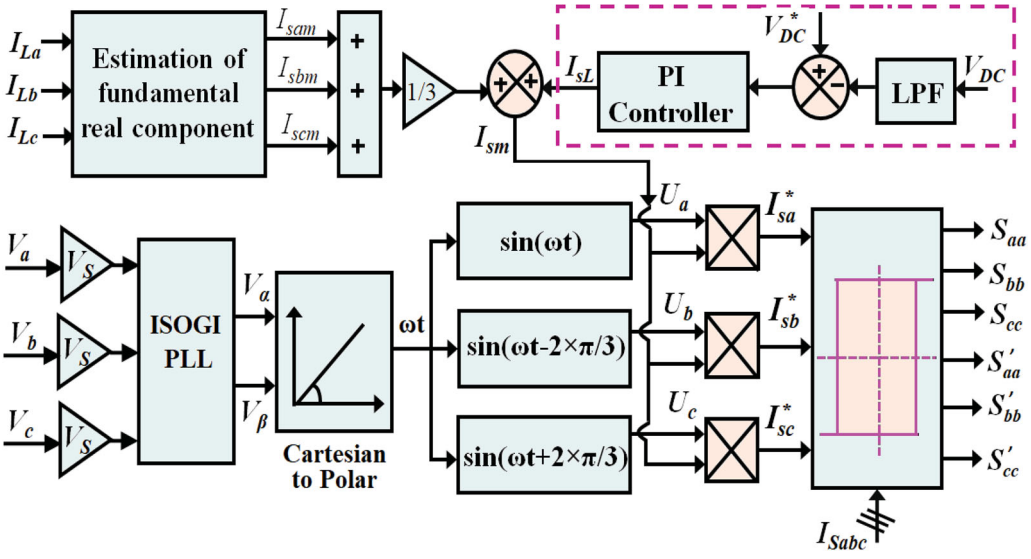


**Figure 6.** The ISOGI PLL based UVT control scheme for shunt compensator.

value of $k$ must be properly quantified which defines the device response time constant. The series or shunt compensator is synchronized with the grid using this PLL, which determines the transformation angle. Using the transition angle, unit templates are generated by the UVTG technique to generate a reference signal for both series and shunt compensators.

### 3.1. Shunt compensator control

Figure 6 shows an ISOGI PLL based UVT control scheme for shunt compensator. The shunt compensator detects the load current and injects the compensation current into the device to alleviate for the current distortions or reactive load. The current reference

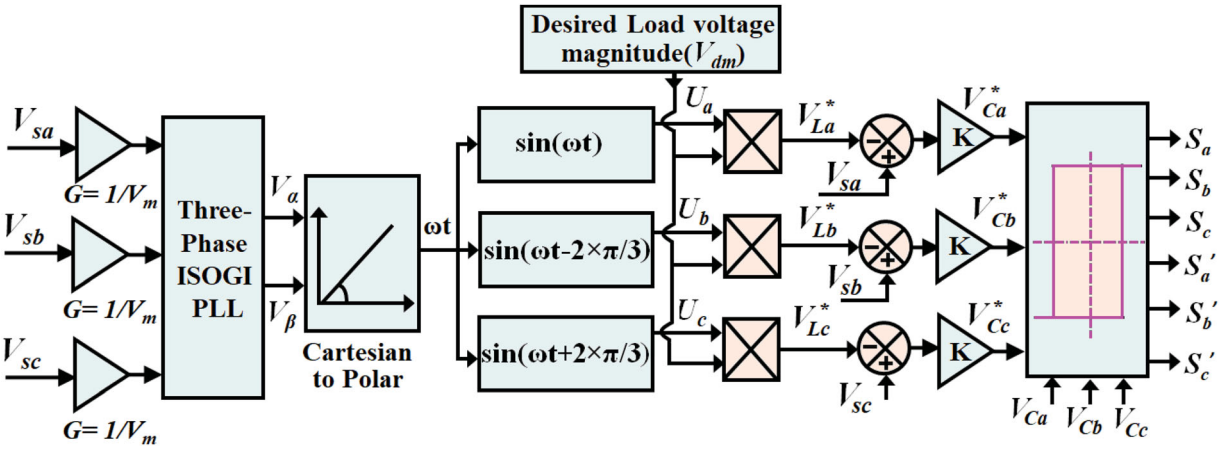


**Figure 7.** SOGI PLL based UVT control scheme for PV-DVR.

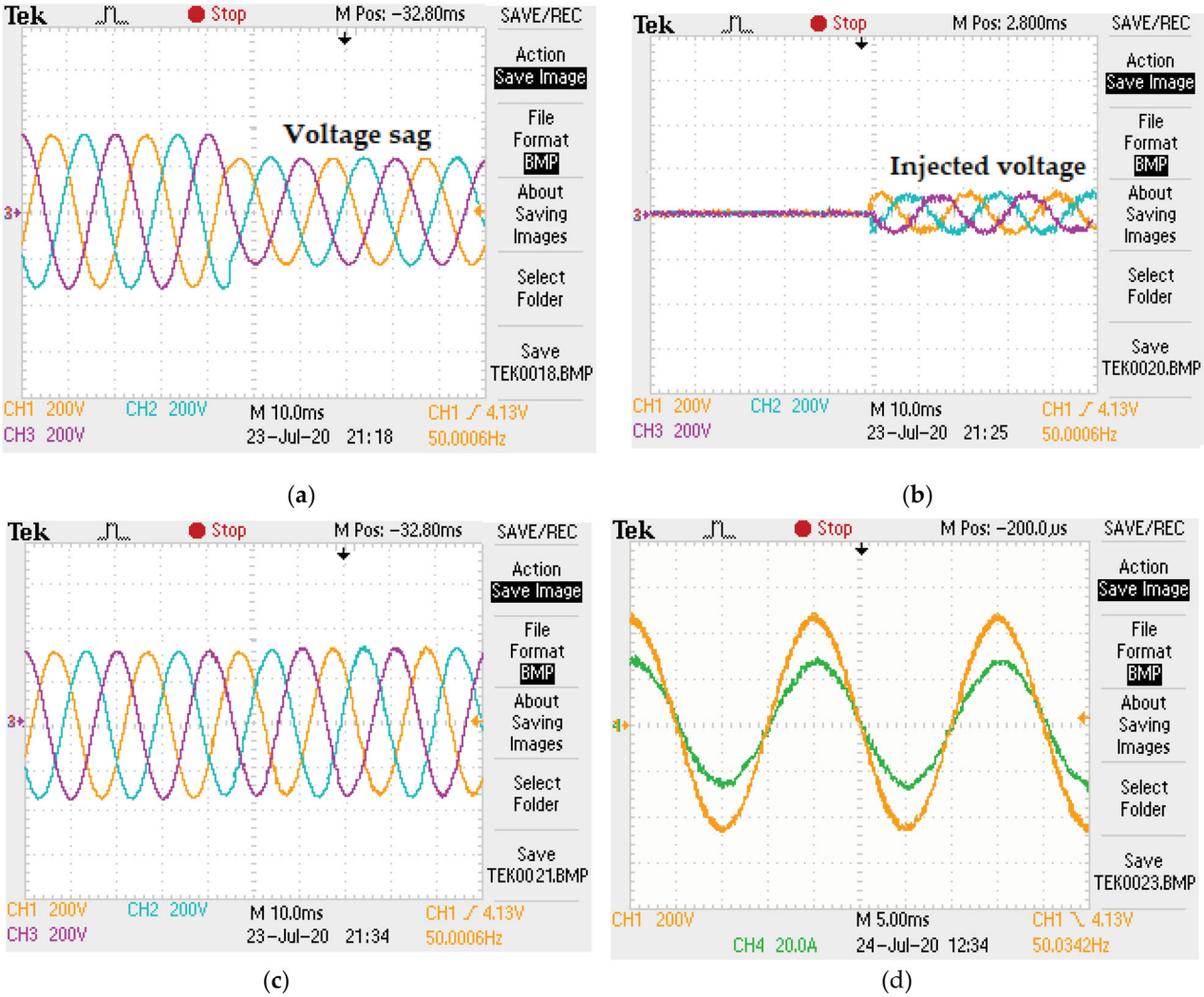


**Figure 8.** (a) balanced grid supply voltage (b) series compensator voltage (c) voltage of the load point (d) grid voltage and current.

signals are necessary for the estimation of the compensation current[23]. The non-linear load is associated to the network in such a way that the device impedance offers distorted load current and voltages at the load point. Equation (3) determines the instantaneous load current.

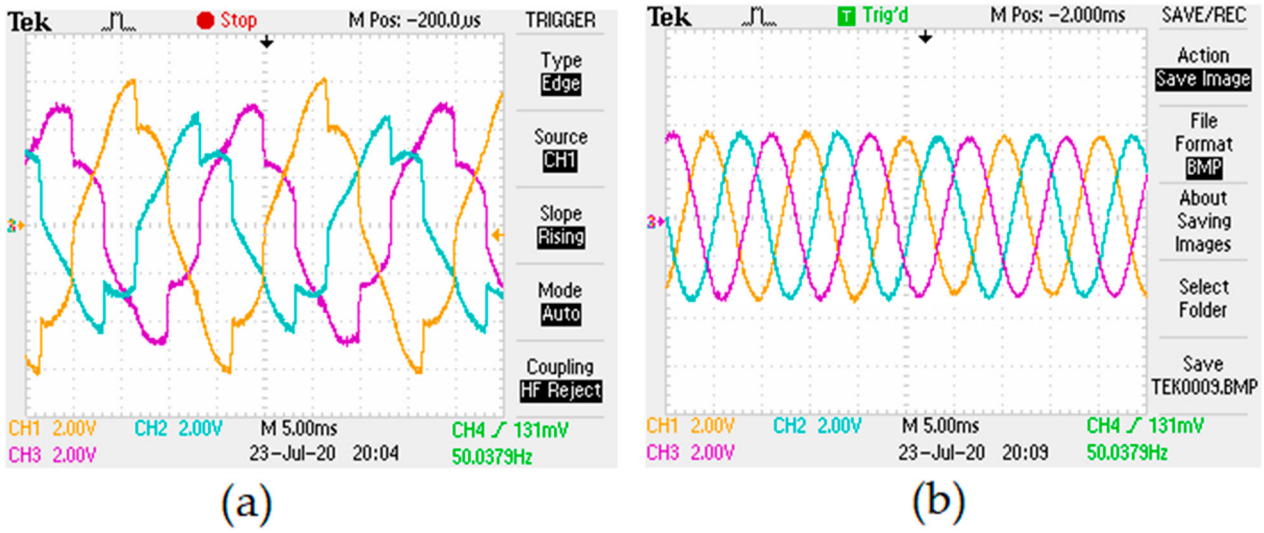


**Figure 9.** (a) Unbalanced distorted grid current (b) grid current after compensation.

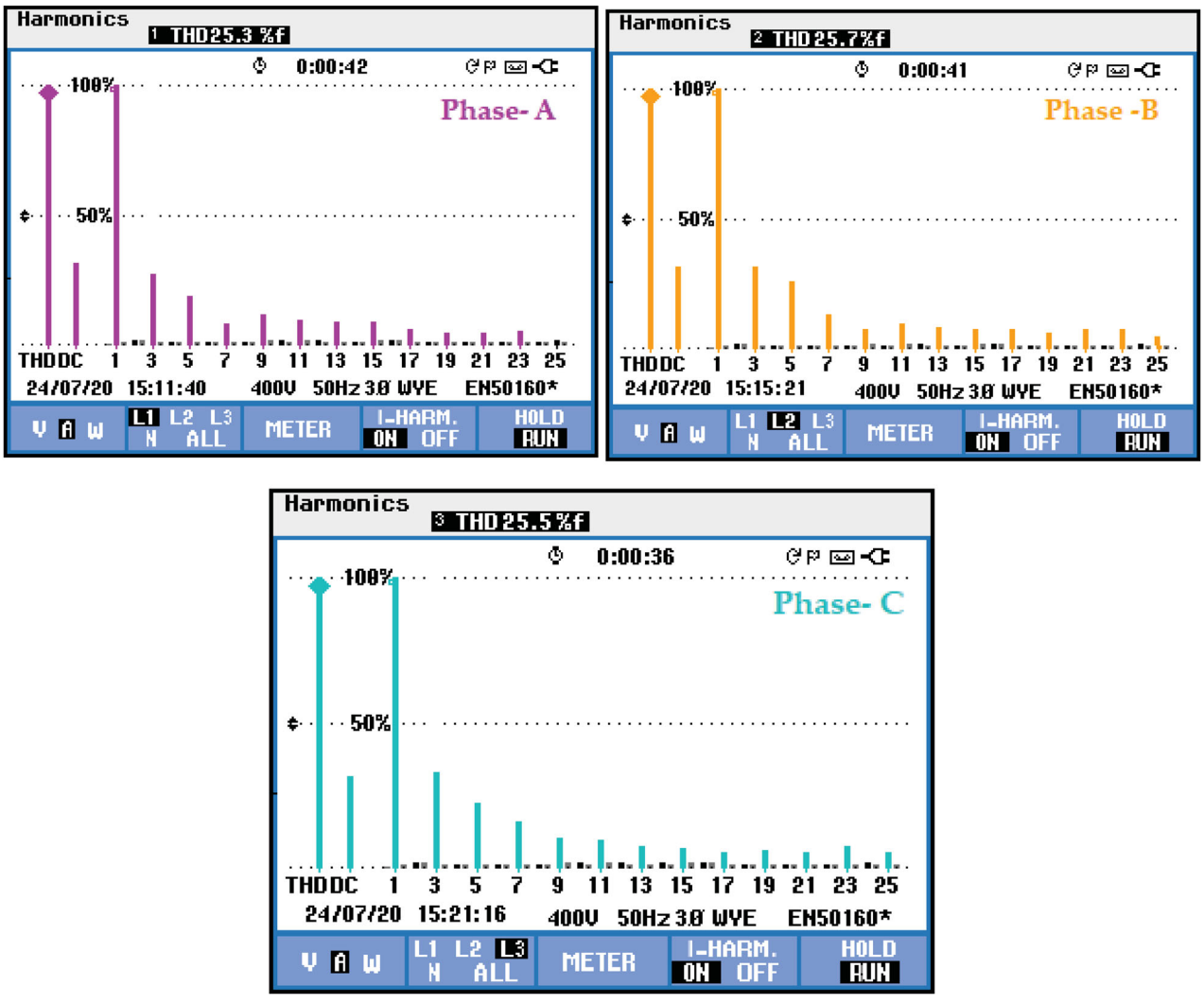


**Figure 10.** Harmonic distortions of the load current before installation of SPV-based ZSI-UAPF in the phases *a*,*b* and *c*.

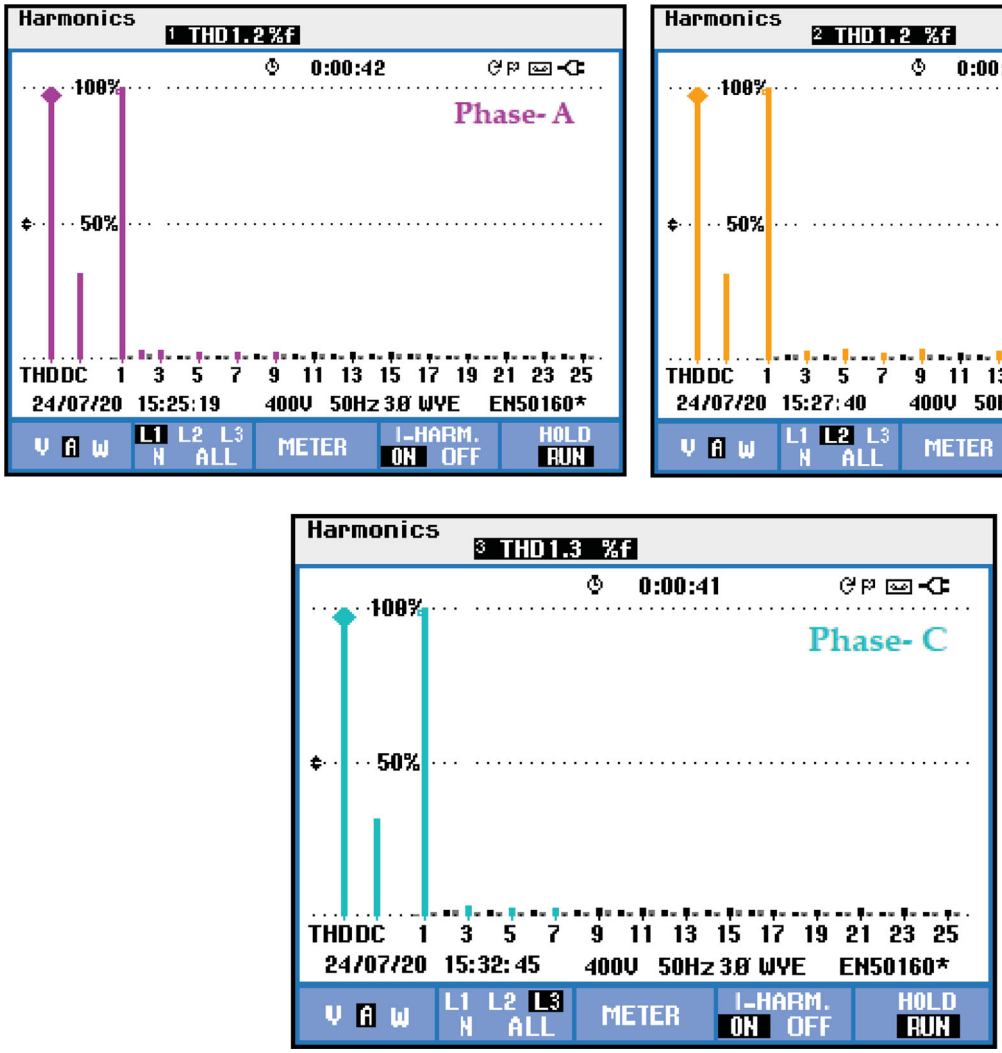


**Figure 11.** The source current harmonic distortions after installation of the SPV backed ZSI-UAPF.

$$i_{Lx} = I_{Lx1} \sin(wt - \phi_{x1}) + \sum_{n=2}^{\infty} I_{Lxn} \sin(n\,wt - \phi_{xn}) \tag{3}$$

Let $x$ be the defined phase ($x = a$, $b$ and $c$). The fundamental true components of the source current after compensation are computed by the Equations (4)–(6).

$$I_{sam} = |I_{La1}| \cos \phi_{a1} \tag{4}$$

$$I_{sbm} = |I_{Lb1}| \cos \phi_{b1} \tag{5}$$

$$I_{scm} = |I_{Lc1}| \cos \phi_{c1} \tag{6}$$

The SPV-UAPF DC-link voltage can vary from its specified magnitude due to switching losses, filter failure and load variations[24]. Designed to retain the UAPF's DC-link voltage at its reference magnitude, the DC-link voltage controller. The voltage controller output is where $I_{SL}$. The maximum value of the source current can be represented in a balanced system by Equation (7).

$$I_{sm} = \left(\frac{I_{sam} + I_{sbm} + I_{scm}}{3}\right) + I_{SL} \tag{7}$$

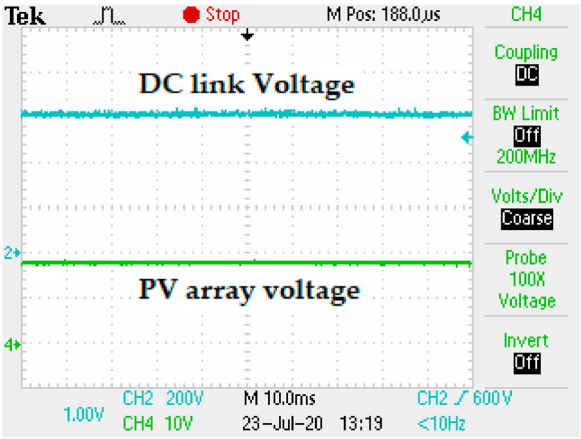


**Figure 12.** ZSI-UAPF DC-link voltage and output voltage of the PV array.

The reference source current must be sinusoids to alleviate current distortions and as the similar value as $I_{Sm}$. The unit vector ($U\,pa$, $U\,pb$, $U\,pc$) is determined using a unit vector template [13]. Equation (8) is indicating the DC-link voltage error at $n^{th}$ instant of

sampling.

$$V_{DCe(n)} = V^{*}_{DCe(n)} - V_{DC(n)} \tag{8}$$

In the $n^{th}$ sample instant, the Proportional Integral(PI) controller output is calculated by Eq.(9).

$$I_{m(n)} = I_{m\,(n-1)} - K_{PV_{DC}}(V_{DCe\,(n)} - V_{DCe\,(n-1)}) + K_{IV_{DC}}\, V_{DCe\,(n)} \tag{9}$$

The maximum value of grid current compounded by UVT to enable the grid current in phase with the grid supply voltage[25]. Equations (10)–(12) are determines the instantaneous reference source currents.

$$I^{*}_{sa} = I_{sam}\ \sin \omega t \tag{10}$$

$$I^{*}_{sb} = I_{sbm}\ \sin\left(\omega t - \frac{2\pi}{3}\right) \tag{11}$$

$$I^{*}_{sc} = I_{scm}\ \sin\left(\omega t + \frac{2\pi}{3}\right) \tag{12}$$

Let $I^{*}_{sa}$, $I^{*}_{sb}$ and $I^{*}_{sc}$ are indicates the reference source currents (A), $K_{PVDC}$ and $K_{IVDC}$ are represents the PI-based DC-link voltage regulator proportional and integral gains and $I_{sam}$, $I_{sbm}$ and $I_{scm}$ are indicate the maximum source currents (A).

Hysteresis controllers are used for the generation of PWM. It is a feed-back controller that establishes the switching logic. To apply this logic, the hysteresis controller is used to assign two bands of the reference signal, for instance, for the comparison three-phase current signal, the upper $(I^{*}_{sa} + h1)$ and lower $(I^{*}_{sa} - h1)$bands. Then by using the following logic switches of $a$-phase leg of VSI controlled as follows:

If $I_{Sa} \leq I^{*}_{Sa} - h_1$, top switch $(S_{aa})$ of leg "$a$" is turned ON and the bottom switch $(S^{'}_{aa})$ of this leg is OFF.

else if $I_{Sa} \geq I^{*}_{Sa} + h_1$, top switch $(S_{aa})$ of leg "$a$" is turned OFF and the bottom switch $(S^{'}_{aa})$ of this leg is ON.

Both the status of the top and bottom switch is complementary with the assistance of NOT gate, two PWM signals are obtained. Consequently, PWM signals are produced for two other phases $b$ and $c$.

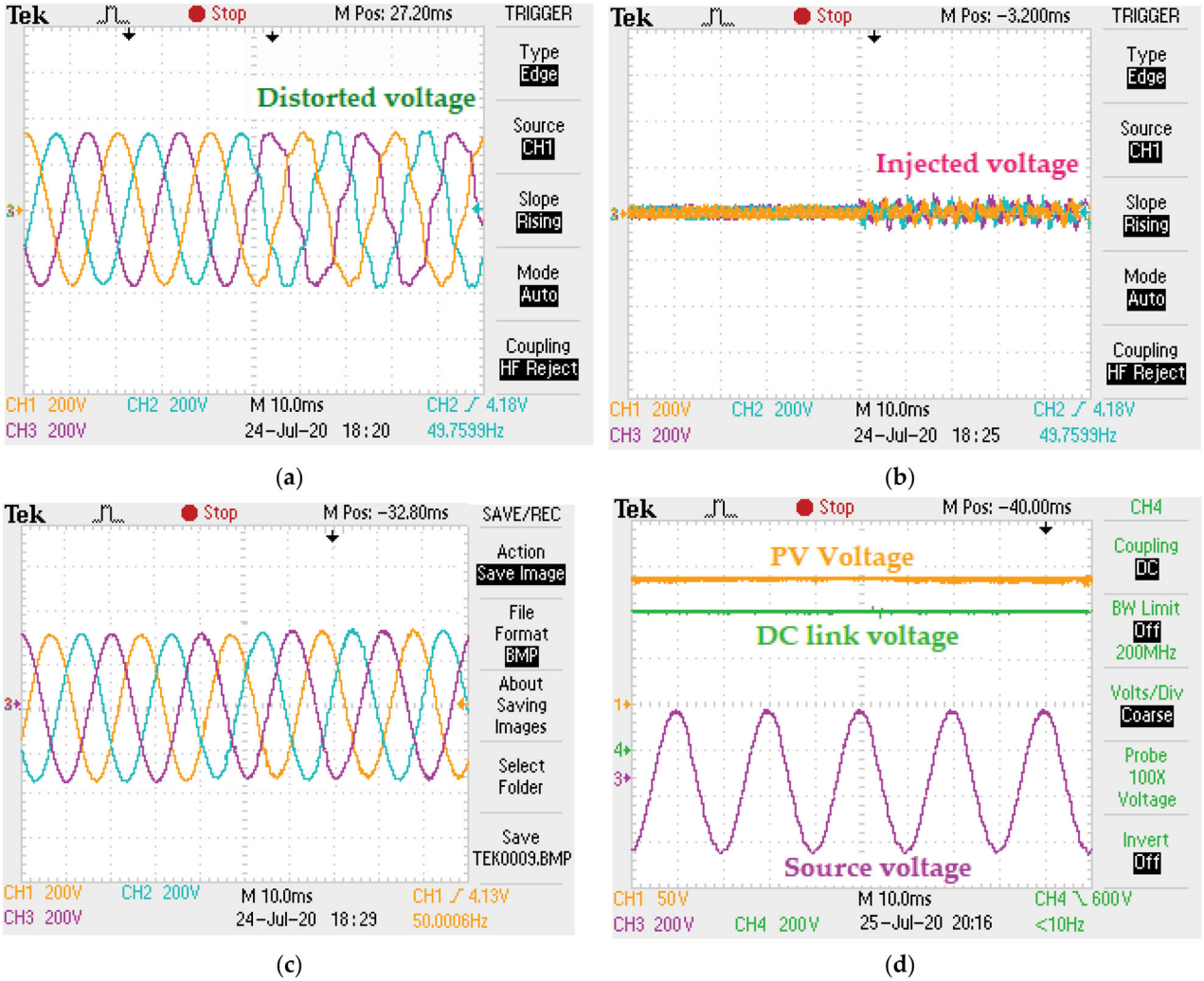


**Figure 13.** Experimental study results: (a) distorted grid supply voltage (b) series compensator injected voltage (c) load point voltage (d) PV array, DC-link and source voltages.

### 3.2. Series compensator control

Figure 1 shows the UVT control scheme based on SOGI PLL for DVR reference voltage production[26]. The measured distorted source voltage, which is equal to $(1/V_m)$, is multiplied by the gain $(G)$. The peak amplitude is calculated with the Equation (13) for fundamental source voltage $(V_m)$.

$$Vm = \sqrt{2/3}\sqrt{V_{sa}^2 + V_{sb}^2 + V_{sc}^2} \tag{13}$$

The approximated peak of the fundamental source voltage is transferred to SOGI PLL. SOGI-PLL has the main function of preserving synchronization with the source voltage and generating unit vectors. The orthogonal signal is produced by SOGI PLL. The orthogonal signal is transformed by the Cartesian to the Polar block in a polar coordinated frame. The required correction of the phase is obtained from the sin generator Figure 7.

The Equation (14) derives the unit vectors.

$$\left.\begin{aligned} U_a &= \sin(\omega t) \\ Ub &= \sin\left(\omega t - 2\frac{\pi}{3}\right) \\ Uc &= \sin\left(\omega t + 2\frac{\pi}{3}\right) \end{aligned}\right\} \tag{14}$$

It is intended that the reference load voltage is strictly sinusoidal, with the magnitude of the required load voltage $(V_{dm})$ and therefore in phase with the source current, in order to get optimal compensation. Then, the desired load voltage $(V_{dm})$ value is multiplied by the unit vector, the source current being in phase. Eq.(15) estimates the reference voltage of the load.

$$\begin{bmatrix} V_{La}^* \\ V_{Lb}^* \\ V_{Lc}^* \end{bmatrix} = [V_{dm}] \begin{bmatrix} U_a \\ U_b \\ U_c \end{bmatrix} \tag{15}$$

In Equations (16)–(18) are presented the individual load reference voltage.

$$V_{La}^* = V_{dm}\, U_a = V_{dm} \sin \omega t \tag{16}$$

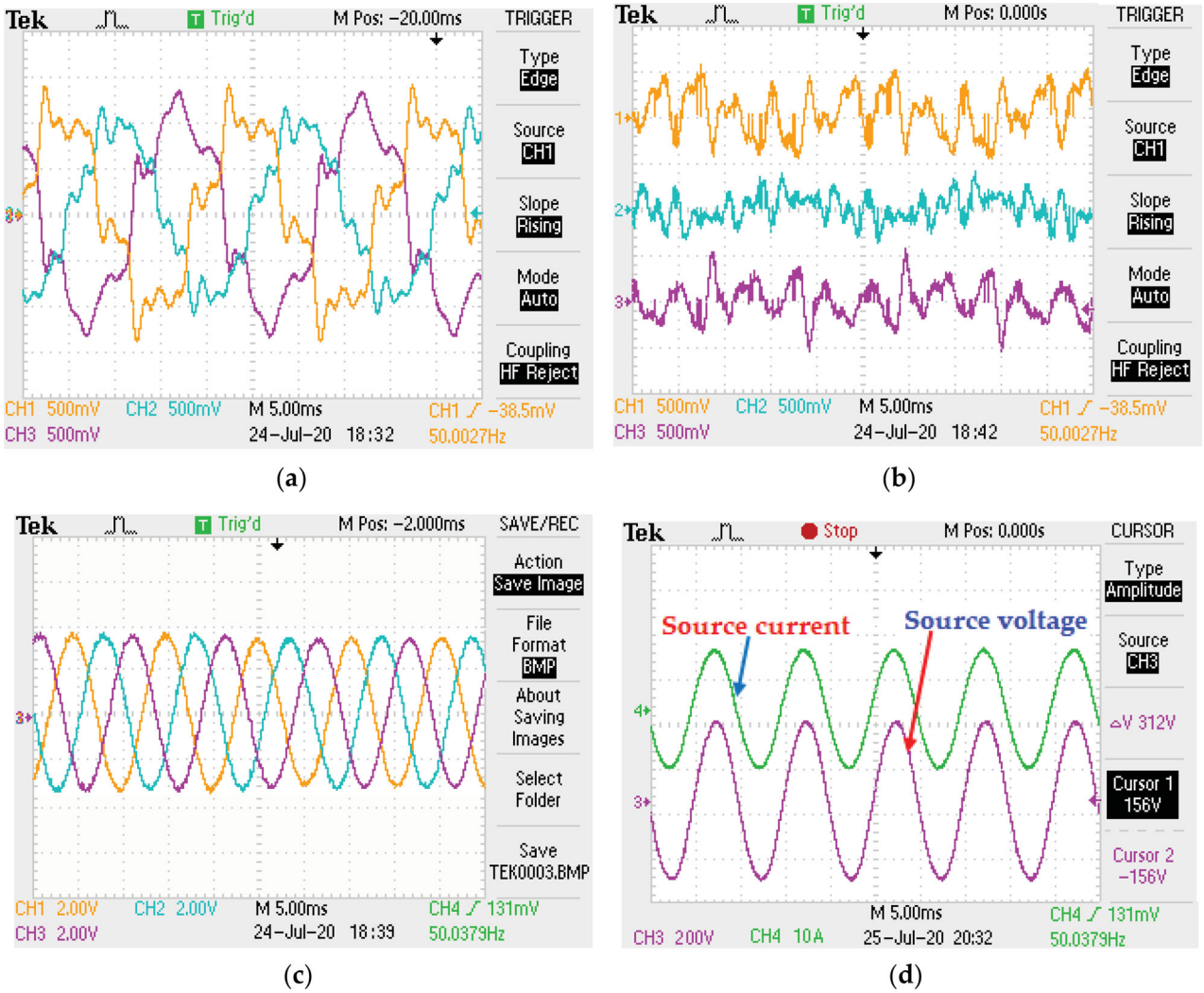


**Figure 14.** Current compensation outcomes of experimental study: (a) unbalanced load current (b) shunt compensator injected current (c) grid current after installation of UAPF circuitry (d) source current and voltage.

$$V_{Lb}^{*} = V_{dm}\, U_b = V_{dm} \sin\left(\omega t - 2\frac{\pi}{3}\right) \quad (17)$$

$$V_{Lc}^{*} = V_{dm}\, U_c = V_{dm} \sin\left(\omega t + 2\frac{\pi}{3}\right) \quad (18)$$

To implement this logic, two bands of the reference signal is fixed by using hysteresis, for an example, for – phase reference current signal, the upper band $V_{La}^{*} + h_2$is and lower band is $V_{La}^{*} - h_2$. Then by using the following logic switches of *a*-phase leg of VSI controlled as follows

If $V_{La} \leq V_{La}^{*} - h_2$, top switch $(S_a)$ of leg "*a*" is switched ON and the bottom switch $(S_a^{'})$ of this leg in OFF.

else if $V_{La} \geq V_{La}^{*} + h_2$, top switch $(S_a)$ of the leg "*a*" is switched OFF and bottom switch $(S_a^{'})$ of this leg in ON.

The estimated voltage of reference load $(V_{La}^{*}, V_{Lb}^{*}, V_{Lc}^{*})$ is compared to three-phases source voltages calculated $(V_{sabc})$ and substituted by the series injection transformer transformation ratio (K) and generating the reference compensator voltages $(V_{CLa}^{*}, V_{CLb}^{*}, V_{CLc}^{*})$. The hysteresis voltage controller may be used to produce the pulses to the ZSI by utilizing the reference voltage of the compensator and the measured output voltage of the series compensator.

## 4. Experimental results and discussion

The PV-UPQC output is tested by the experimental prototype by utilizing the UVTG technique with ISOGI based PLL. This paper addresses issues with power quality such as voltage sag, voltage swell, voltage and current distortions. Both the series and shunt inverters are connected back to back through the Z-source network. The three-phase source is connected to the linear load and nonlinear loads such as three-phase Resistive (R)-Inductive (L) load and three-phase diode bridge rectifier supplying a resistive load and inductive load respectively. The series inverter of ZSI based PV-UAPF is connected to the power network through three single-phase transformers at the source side. The shunt inverter is connected in parallel at the load side through a coupling inductor. FPGA processor has been employed for the control of ZSI based PV-UAPF by sending switching signals. Hall effect transducers have

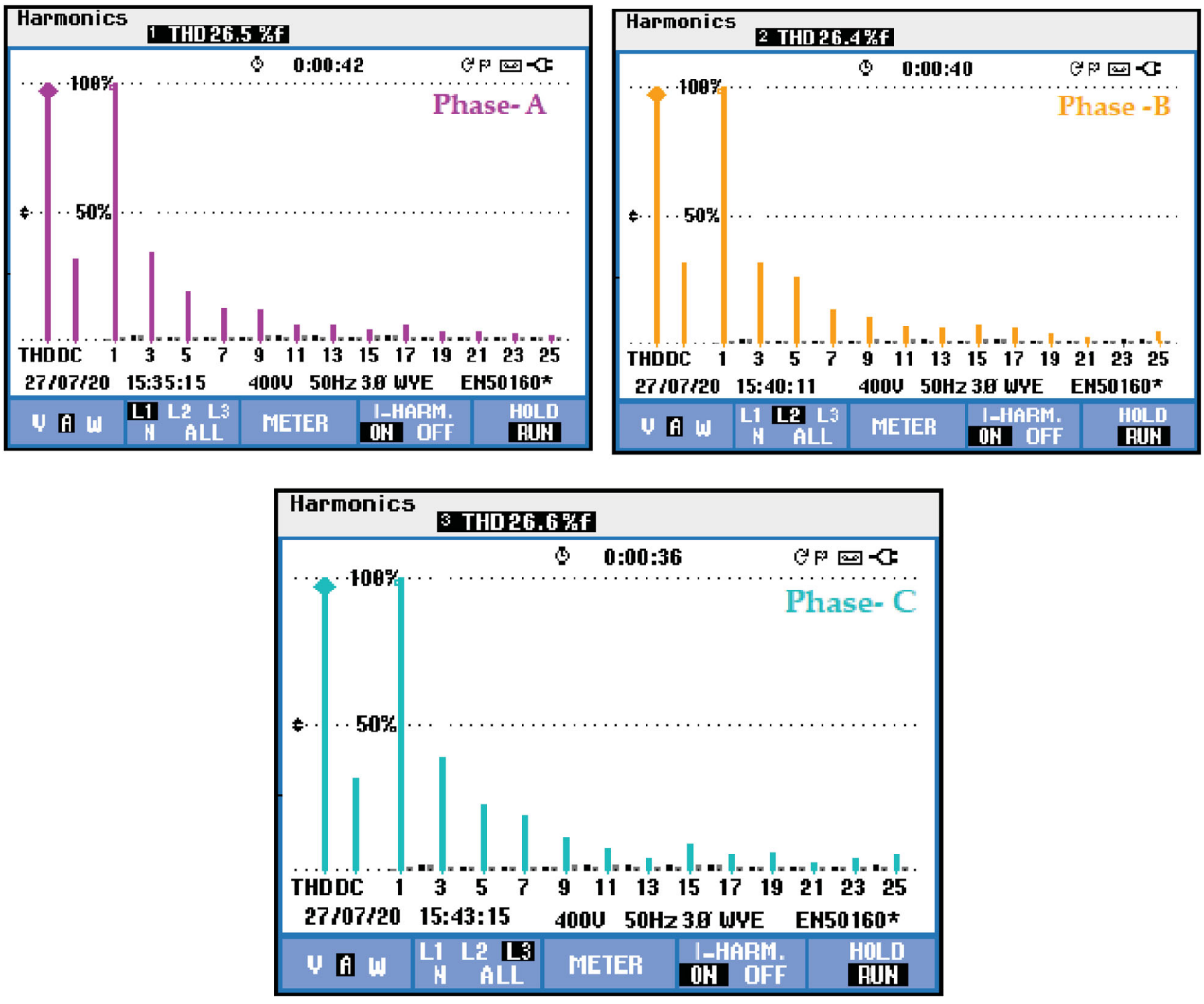


**Figure 15.** Load current THD level without harmonic compensation in phases *a*,*b* and *c*.

been used for current and voltage sensing of the system. Experimental results have been analysed to validate the efficiency of ZSI based PV-UAPF. Three different instances have been studied: balanced voltages with an unbalanced load, distorted voltages with unbalanced load and unbalanced grid supply voltages with an unbalanced load.

### 4.1. Performance of ZSI based PV-UAPF under balanced supply voltages with an unbalanced load

This section describes the performance of ZSI-based PV-UAPF with balanced voltages of supply with an unequalled load. The tests are carried out at 230V (Line-Neutral, r.m.s.). The DC-link is powered with a PV system and maintained at 600V. The balanced grid supply voltage, series compensator voltage, the voltage of the load point and grid voltage and current are shown in Figure 8. The voltage sag is detected by the ZSI-UAPF with ISOGI based PLL and injects an appropriate compensation voltage and alleviate the balanced voltage sag. Figure 9 shows the experimental outcomes of unbalanced distorted and grid current after compensation. The shunt compensator compensates the grid current after injecting a sufficient compensation current and adjusts the grid current to be sinusoidal after compensation.

Before and after the installation of ZSI-UAPF, harmonic distortions are tracked to evaluate the compensation ability of the ZSI-UAPF. The harmonic distortions of the load current before installation of SPV based ZSI-UAPFis shown in Figure 10.

Figure 11 shows the source current harmonic distortions after installation of the SPV backed ZSI-UAPF. The average THD level of source is reduced to 1.2(%) which is less than the THD level specified by the IEEE-519-1992 Standard. Figure 12 shows the PV array output voltage and the DC-link voltage of the ZSI-UAPF. For efficient compensation of current and voltage distortion, ZSI-UAPF DC bus voltage must be sustained at a constant voltage.

### 4.2. Performance of ZSI based PV-UAPF under distorted voltages with an unbalanced load

The efficiency of the PV assisted ZSI-UAPF is investigated with unbalanced load in distorted voltages. The distorted grid supply voltage, series compensator injected voltage, the voltage of the load point and PV array, DC-link and source voltages are shown in

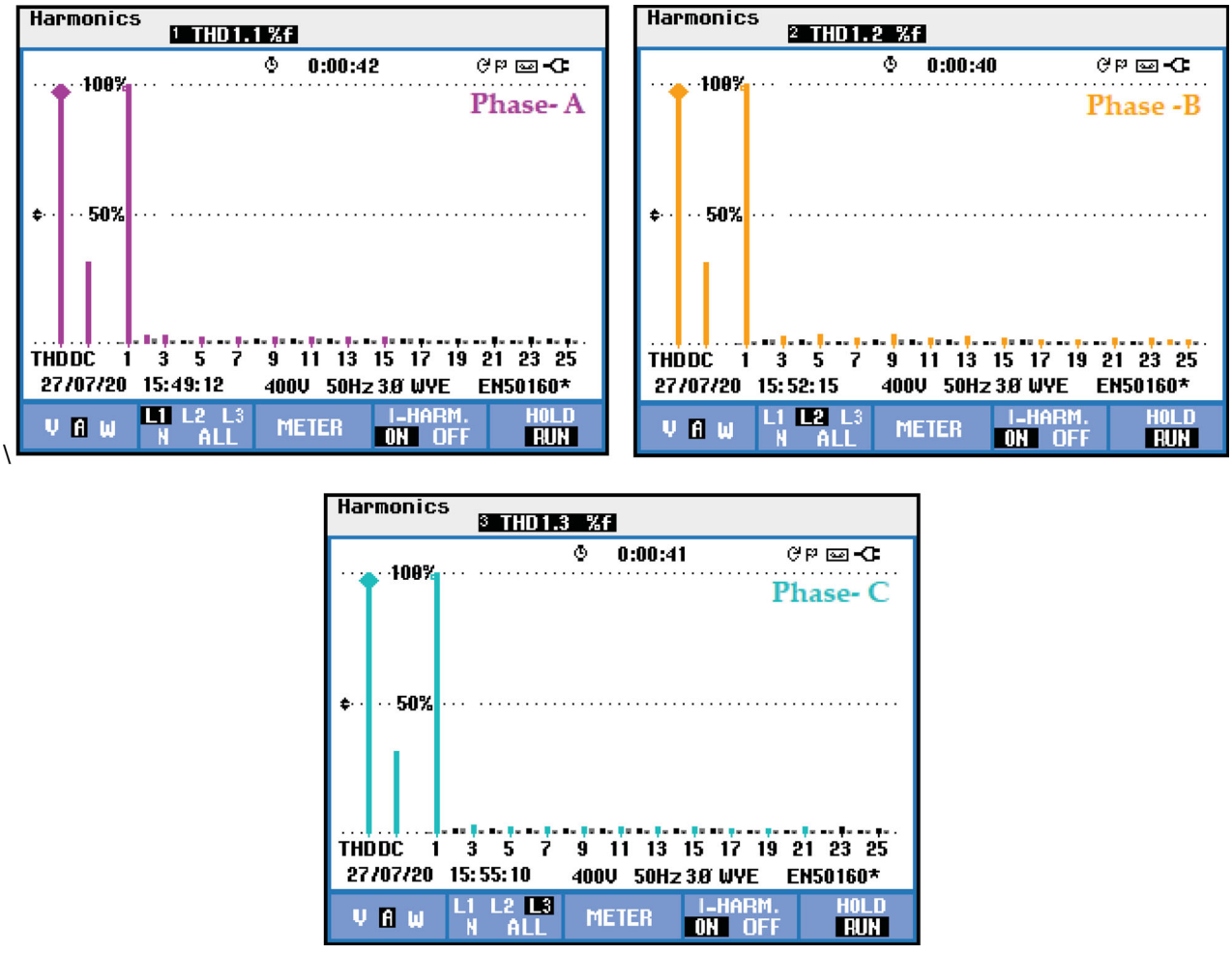


**Figure 16.** Source current THD level with harmonic compensation in phases *a*,*b* and *c*.

Figure 13. An unbalance created by the attachment of three single-phase bridge rectifiers in the non-linear load. Figure 14 shows the unbalanced load current, shunt compensator injected current, grid current after installation of UAPF circuitry and source current and voltage. Since a balanced three-phase reference is being tracked continuously, the UAPF forces the source current to be sinusoidal and balanced. The shunt compensator supplies the rest of the current to the load as required by the load.

The load current THD values (in %) are observed as high as 26.5,26.4 and 26.6, respectively, without harmonic compensation. Figure 15 shows the load current THD level without harmonic compensation.

However, these values are regulated to 1.1,1.2 and 1.3, respectively, with harmonic compensation. Figure 16 shows the source current THD level with harmonic compensation. The harmonics in series compensator output voltage are precisely controlled to compensate for the harmonic currents entering the grid. The average THD of grid current is regulated to 1.2% even with nonlinear load current THD of 26.5%, as the harmonic control is enabled with the use of ZSI-UAPF.

### 4.3. Performance of ZSI based PV-UAPF under unbalanced grid supply voltages with unbalanced loads

The test is performed under unbalanced grid supply voltages with unbalanced load currents. The unbalanced voltage sag and swell are applied to test the voltage compensation. The compensation voltage injects the series compensator when the voltage sag and swell is observed by the PV backed ZSI-UAPF. Figure 17 displays the unbalanced grid voltage, voltage of series compensator and voltage of the load point.

Figure 18 shows the unbalanced load current, grid current after installation of ZSI-UAPF circuitry, PV array, DC-link and source voltages. As a balanced three-phase reference is constantly monitored, the ZSI-UAPF imposes a sinusoidal and balanced source current.

This segment presents the performance of the PV supported ZSI-UAPF during abrupt load changes.

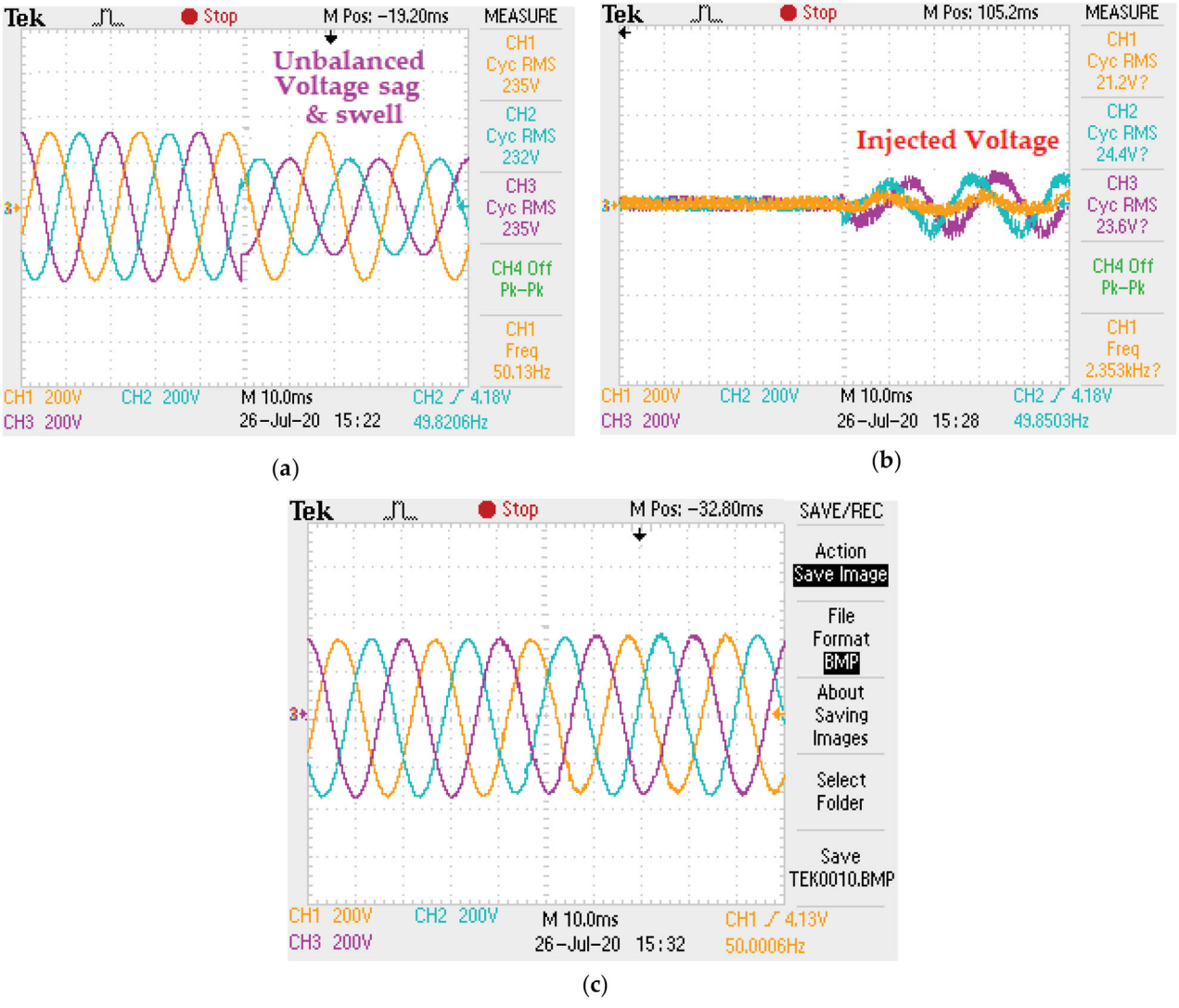


**Figure 17.** (a) unbalanced grid voltage (b) series compensator injected voltages (c) voltage of the load point.

Figures 19(a) and (b) demonstrate the dynamic characteristics of the DC-link voltage during nonlinear load switching. By the operation of the PI controller, the DC-link voltage is maintained at 600V. The real power supplied to the load is previously passed on to a DC-link capacitor while the nonlinear load is shut down before a new grid reference current is suitable for a new load current will be estimated. The voltage of the DC-link thus exceeds the reference value. Similarly, if a load is turned on, the DC-link voltage decreases. To balance the DC-link voltage, the controller takes several power cycles. Figures 19 show the source voltage, load current and DC – link voltage during switch on and switch off a non-linear load respectively.

Without harmonic compensation, the value of THD (in %) load current is observed as high as 26.8,26.5 and 26.9. The load current THD level without harmonic compensation is shown in Figure 20. These THD values are reduced to 1.2,1.2 and 1.3 respectively with the harmonic compensation. The source current THD level with harmonic compensation is shown in Figure 21. The harmonics are precisely regulated with the series compensator output voltage to compensate for the harmonic currents in the grid. Even with nonlinear load current THD of 26.7%, the average THD of grid current is reduced to 1.2%, as harmonics compensation with the use of ZSI-UAPF.

The consumed load active power and reactive power during the unbalanced grid supply voltage and load current condition is shown in Figure 22. The active power of the load is supplied by the utility grid and power generated from the PV power generating systems. The reactive power demand compensated by the shunt compensator of the ZSI-UAPF.

The feasibility of the system proposed has been examined in various instances. For the proposed system an experimental prototype model is designed to validate the use of the PV-supported ZSI-UAPF for compensating distortion depends on voltage and current. The ZSI-UAPF compensation ability is determined by the percentage of the THD level. Figure 23 indicates the current harmonics THD values for with and without

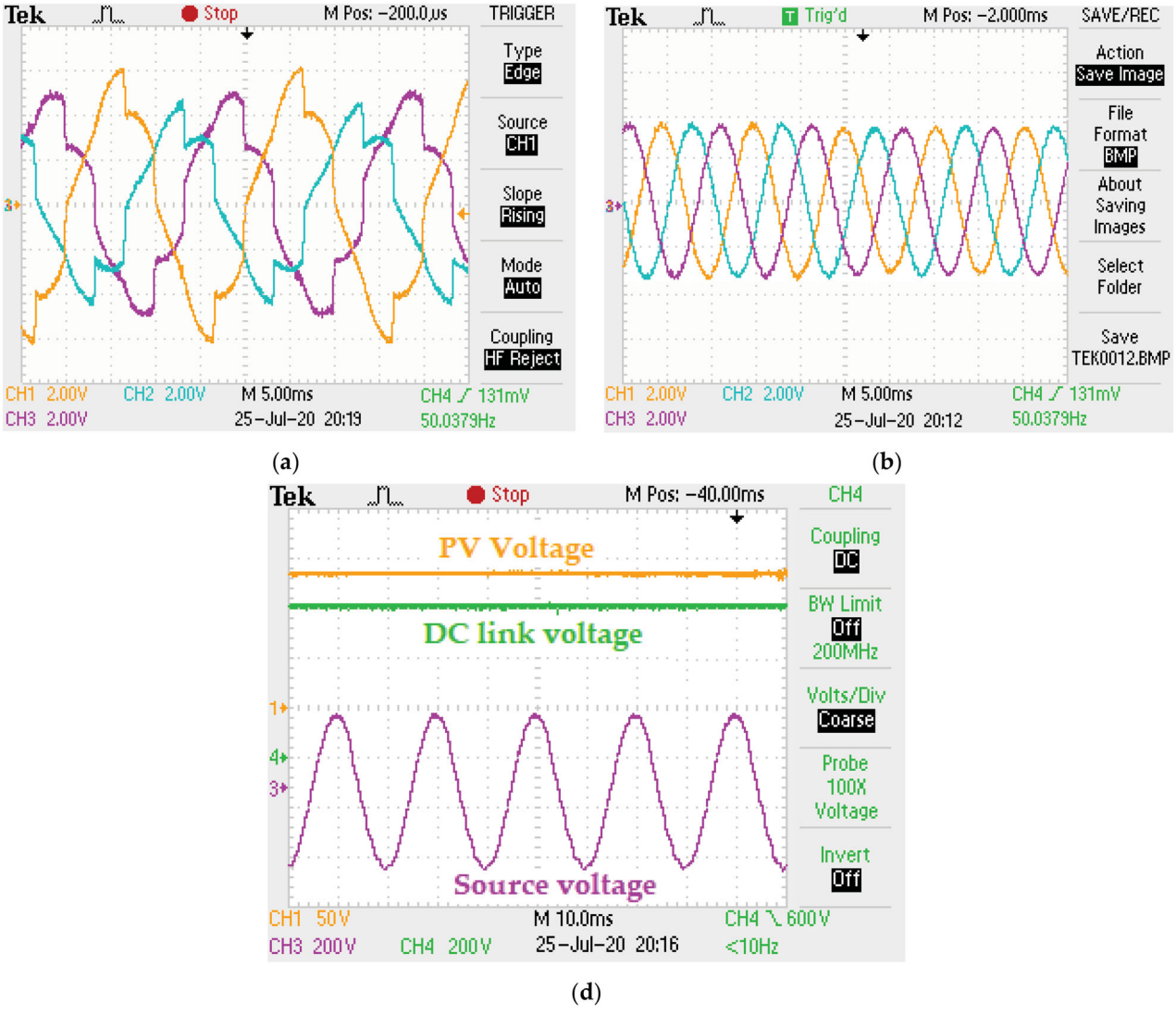


**Figure 18.** Experimental output waveforms: (a) unbalanced load current (b) grid current after installation of ZSI-UAPF circuitry (d) PV array, DC-link and source voltages.

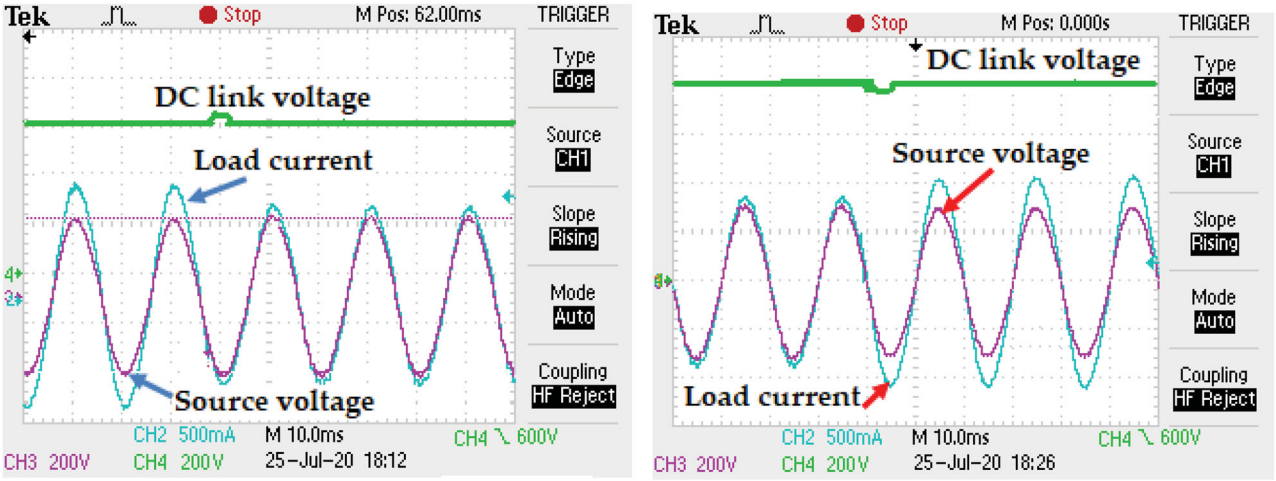


**Figure 19.** DC-link voltage control results: (a) DC – link voltage during switch on and switch off a non-linear load (b) DC – link voltage during switch on and switch on a non-linear load.

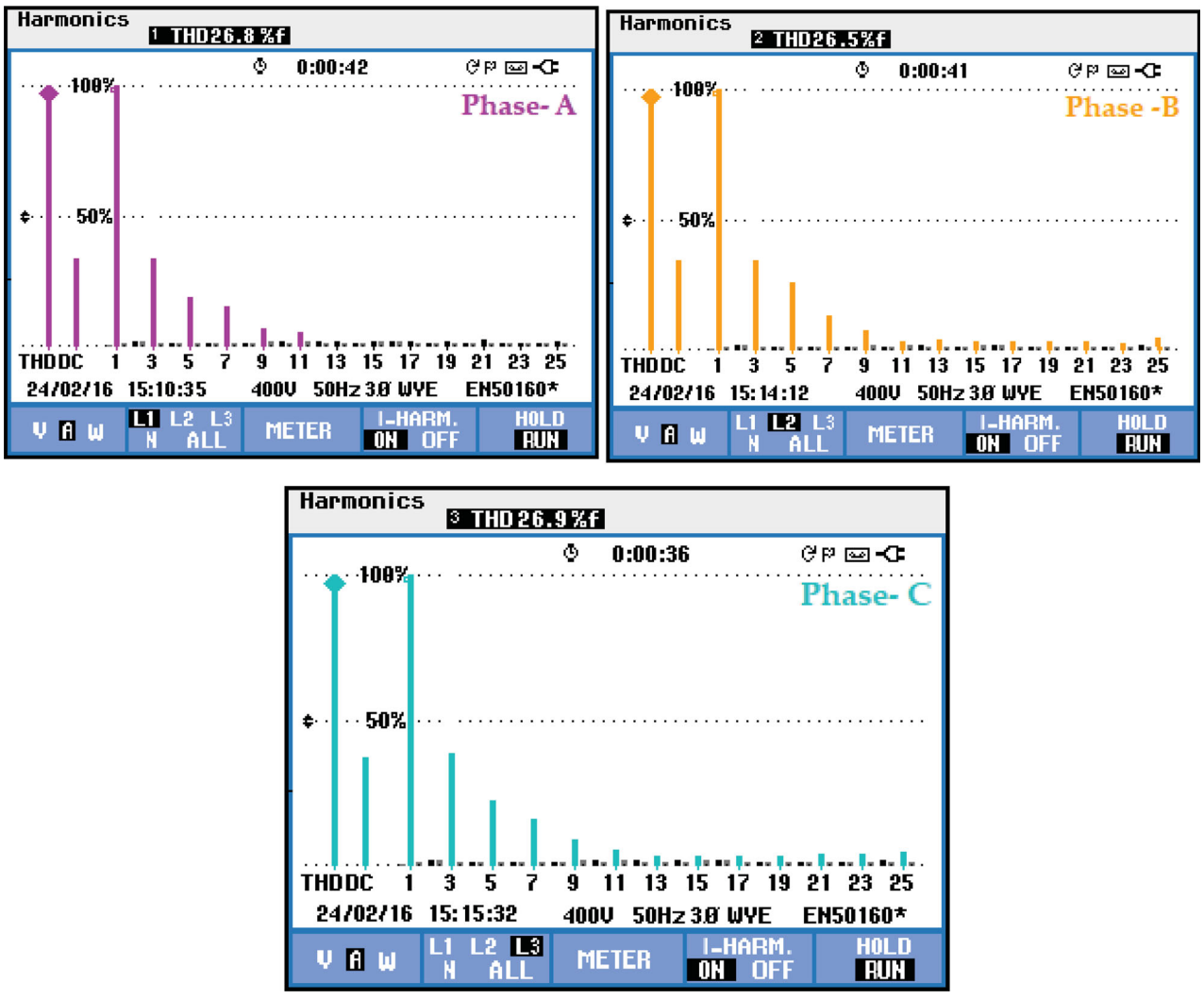


**Figure 20.** Load current THD level without harmonic compensation in phases *a*,*b* and *c*.

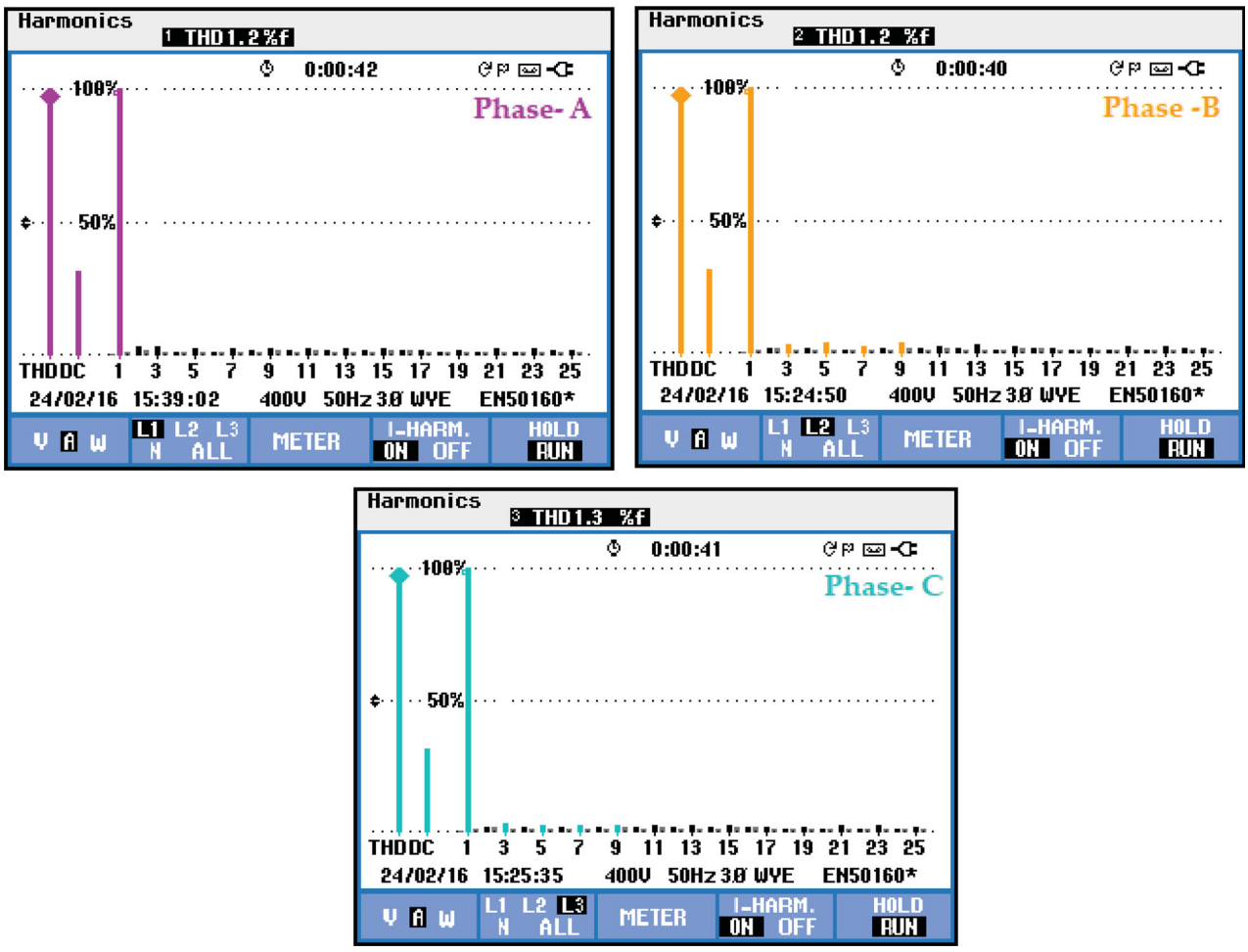


**Figure 21.** Source current THD level with the harmonic compensation in phases *a*,*b* and *c*.

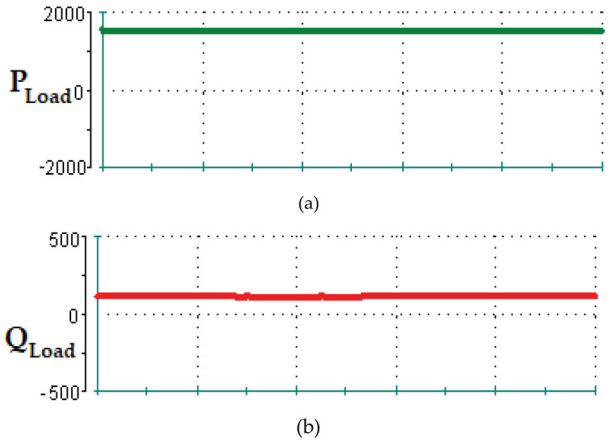


**Figure 22.** Experimental study under the unbalanced grid supply voltage and load current:(a) load active power (b) load reactive power.

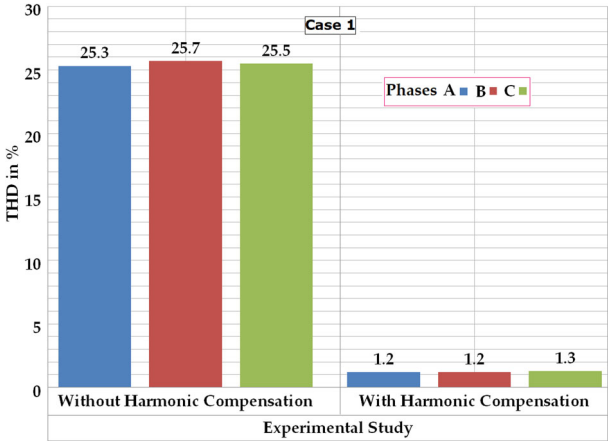


**Figure 23.** Current harmonics THD values for with and without harmonic compensation under unbalanced load conditions with balanced voltages.

harmonic compensation under unbalanced load conditions with balanced voltages.

The current harmonics THD levels for with and without harmonic compensation under unbalanced load conditions with distorted voltages is shown in Figure 24. Figure 25 shows the current harmonics THD values for with and without harmonic compensation under unbalanced load conditions with unbalanced voltages.

The source current THD level after compensation is considerably less about 1.2(%) in the presented PV assisted ZSI UAPF under unbalanced, non-linear load conditions. Compared to conventional topology with THD levels were 4.77(%) as documented by Mansor

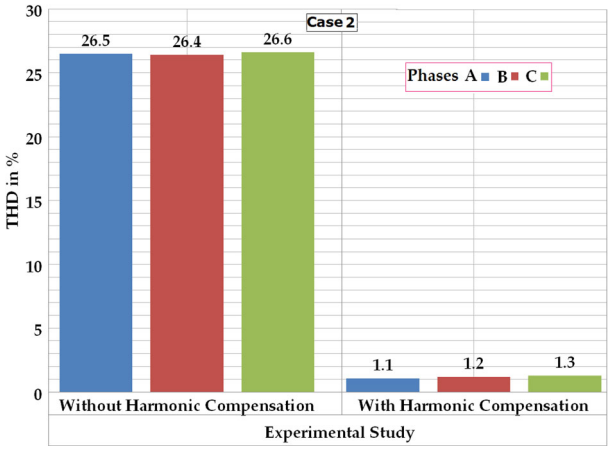


**Figure 24.** Current harmonics THD levels for with and without harmonic compensation under unbalanced load conditions with distorted voltages.

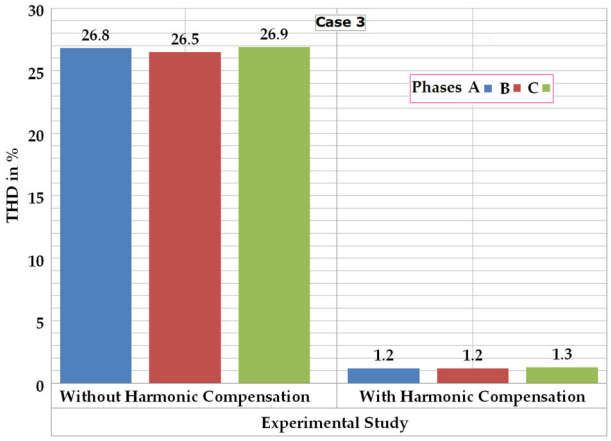


**Figure 25.** Current harmonics THD values for with and without harmonic compensation under unbalanced load conditions with unbalanced voltages.

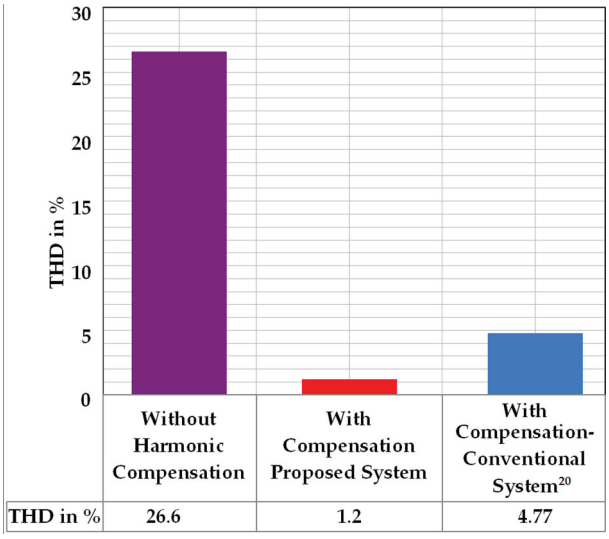


**Figure 26.** current harmonics THD level comparision between the proposed system with conventional system presented by Mansor et al. [20].

et al. [20]. The current harmonics THD level comparision between the proposed system with conventional system presented by Mansor et al. [20] is shown in Figure 26.

## 5. Conclusion

In this article, the UVTG with improved SOGI based PLL is used for ZSI-UAPF to combine PV systems into the utility grid with the enrichment of power quality. To establish reference source current and voltage signals, UVTG is used with improved SOGI-based PLL. In order to provide long-term voltage and current compensation, the green energy generation system holds up the DC bus voltage of the ZSI-UAPF. The topology suggested is provided by reliable energy storage systems such as a battery for the optimal use of solar energy. The excess electricity generated by the PV system is stored in the battery storage system. Thus, the conversion and transformation of the stored energy are carried out with the multi-mode feature. This simple control algorithm has accomplished harmonic mitigation, voltage, and current compensation. The harmonic distortion of the source current in non-linear loads with different current conditions is reduced to approximately 1.2%, below the 8% tolerable limit as defined by the IEEE standard 1547-2018[27]. The test results show that the control and topological efficiency is more efficient in compensating the voltage and current disruptions than any other typical compensating unit.

## Disclosure statement

No potential conflict of interest was reported by the author(s).

## ORCID

*S. Parthiban* http://orcid.org/0000-0001-6775-6804
*Vijayakumar Madhaiyan* http://orcid.org/0000-0001-5224-6983

## References

[1] Aredes M, Heumann K, Watanabe EH. An universal active power line conditioner. IEEE Trans Power Delivery. 1998;13(2):545–551.
[2] Vijayakumar M, Vijayan S. PV based three-level NPC shunt active power filter with extended reference current generation method. International Journal of Electrical Energy. 2014;4:258–267.
[3] Shah P, Hussain I, Singh B, et al. GI-Based control scheme for single-stage grid interfaced SECS for power quality improvement. IEEE Trans Ind Appl. 2019;55:869–881.
[4] Park J, Lee H, Yoon M, et al. A novel method for assessing the contribution of harmonic sources to voltage distortion in power systems. IEEE Access. 2020;8:76568–76579.
[5] Aissa O, Moulahoum S, Colak I, et al. Design and real time implementation of three-phase three switches

three levels Vienna rectifier based on intelligent controllers. Appl Soft Comput. 2017;56:158–172. doi: 10.1016/j.asoc.2017.03.001.
[6] Choudhury SR, Das A, Anand S, et al. Adaptive shunt filtering control of UPQC for increased nonlinear loads. IET Power Electron. 2019;12(2):330–336.
[7] Nieto A, Vita V, Maris TI. Power quality improvement in power grids with the integration of energy storage systems. Int. J. Eng. Res.Technol. 2016;5(7):438–443.
[8] Devassy S, Singh B. Dynamic performance of solar PV integrated UPQC-P for critical loads., in: 2015 *Annual IEEE India Conference (INDICON), IEEE* 2015, 1-6.
[9] Yang M, Tan T, Hu J. Simulation and experiment of algorithm and circuit design for UPQC. Automatika. 2019;60(4):480–490. doi:10.1080/00051144.2019.1645401.
[10] Khadkikar V, Chandra A. A new control philosophy for a unified power quality conditioner (upqc) to coordinate load-reactive power demand between shunt and series inverters. IEEE Trans Power Delivery. 2008;23:2522–2534.
[11] Ebadian M, Talebi M, Ghanizadeh R. A New approach based on instantaneous power Theory for improving the Performance of UPQC under unbalanced and distortional load conditions. Automatika. 2015;56(2): 226–237. doi:10.7305/automatika.2015.07.750.
[12] Shrivastava A, Nene P. Power quality enhancement using UPQC connected with PV arrays, in: Communication Systems and Network Technologies (CSNT). 2015 *Fifth International Conference on, IEEE*, 2015, 1232-1237.
[13] Patel A, Chaturvedi P. Performance of SRF-UVTG based UPQCDG for integration of solar PV with nonlinear loads, in: Power Electronics, Drives and Energy Systems (PEDES), 2016 IEEE International Conference on, IEEE 2016, 1-5.
[14] Vijayakumar M, Vijayan S. Extended reference signal generation scheme for integration of unified power quality conditioner in grid-connected photovoltaic system. Electr Power Compon Syst. 2015;43:914–927.
[15] Jarvela M, Seppo Valkealahti S. Ideal operation of a photovoltaic power plant equipped with an energy storage system on electricity market. Appl. Sci. 2017;7:749. doi:10.3390/app7070749.
[16] Sakar S, Balci ME, Aleem SHA, et al. Integration of large-scale PV plants in non-sinusoidal environments: considerations on hosting capacity and harmonic distortion limits. Renewable Sustainable Energy Rev. 2018;82:176–186.
[17] Vijayakumar M, Vijayan S. A comparative study and implementation of controller for UPQC in single-phase to three-phase system. Int J Eng Tech. 2013;5:3846–3857.
[18] Muthuvel K, Vijayakumar M. Solar PV sustained quasi Z-source network-based Unified power quality conditioner for enhancement of power quality. Energies. 2020;13:2657.
[19] Zhang J. Unified control of Z-source grid-connected photovoltaic system with reactive power compensation and harmonics restraint: design and application. IET Renew Power Gener. 2018;12:422–429.
[20] Mansor MA, Hasan K, Othman MM, et al. Construction and performance investigation of three-phase solar PV and battery energy storage system integrated UPQC. IEEE Access. 2020;8:103511–103538.
[21] Narayanan SK, Sivarajan N, Abdu JE, et al. Integration of solar PV into grid using a new UPQC with differential inverter control. IET Gener Transm Distrib. 2020;14(19):4254–4263.
[22] Devi SC, Singh B, Devassy S. Modified generalised integrator based control strategy for solar PV fed UPQC enabling power quality improvement. IET Gener Transm Distrib. 2020;14(16):3127–3138.
[23] Aissa O, Moulahoum S, Colak I, et al. Analysis and experimental evaluation of shunt active power filter for power quality improvement based on predictive direct power control. Environ Sci Pollut Res Int. 2018;25(25):24548–24560. doi:10.1007/s11356-017-0396-1.
[24] Ferhat M, Rahmani L, Babes B. DSP-based implementation of improved deadbeat control for three-phase shunt active power filters. J. Power Electron. 2020;20:188–197. doi:10.1007/s43236-019-00029-y.
[25] Aissa O, Moulahoum S, Babes B. Functioning ability of multilevel Vienna converter as new parallel active filtering configuration: simulation and experimental evaluation. Electr Eng. 2019;101:1103–1117. doi:10.1007/s00202-019-00856-z.
[26] Xiao F, Dong L, Li L, et al. A frequency-fixed SOGI-based PLL for single-phase grid-connected converters. IEEE Trans Power Electron. 2017;32:1713–1719.
[27] IEEE Standard for interconnection and interoperability of distributed energy resources with associated electric power systems interfaces. IEEE Std 1547-2018, 1-138.

## Appendix

### Experimental parameters

Grid Phase Voltage: 230VRMS; Grid Frequency: 50Hz; DC Bus Voltage:600V; Grid Inductor: 4mH; Filter Parameters: 5mH and 15μF; ZSI Rating: 5kVA; ZSI Switching Frequency ($f_s$): 10 kHz; RL load: R = 20 Ω, L = 0.5mH; Z-source network: L1 = L2 = 160μH, C1 = C2 = 1000μF.